Environmental Science & Technology

pubs.acs.org/est

Article

Mechanistic Study of Ni(II) Sorption by Green Rust Sulfate

Evert J. Elzinga*

Cite This: *Environ. Sci. Technol.* 2021, 55, 10411−10421

Read Online

ACCESS | Metrics & More | Article Recommendations | Supporting Information

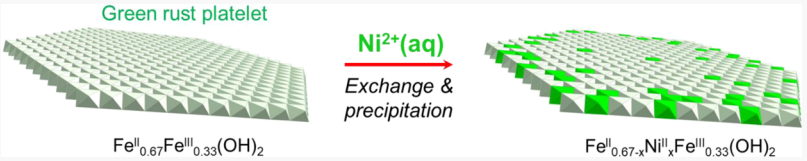

ABSTRACT: The sorption of Ni(II) by green rust sulfate (GR-sulfate) was studied in anoxic pre-equilibrated suspensions at pH 7.0 and pH 7.8 with combined batch kinetic experiments, X-ray diffraction measurements, and Ni K-edge X-ray absorption spectroscopy (XAS) analyses. Continuous removal of aqueous Ni(II) was observed over the course of the reaction (1−2.5 weeks) at both pH values, with no concurrent changes in aqueous Fe(II) levels or detectable mineralogical modifications of the GR sorbent. XAS results indicate that Ni(II) is not retained as mononuclear adsorption complexes on the GR surface but rather incorporated in the octahedral layers of an $Fe^{II}_{0.67-x}Ni^{II}_{x}Fe^{III}_{0.33}(OH)_2$-layered double hydroxide (LDH) phase with $0 < x < 0.67$. The combined macroscopic and spectroscopic data suggest that Ni(II) substitutes into the GR lattice during Fe(II)-catalyzed recrystallization of the sorbent and/or forms secondary Ni(II)/Fe(II)−Fe(III)-LDH phases with a higher stability than that of GR, complemented likely by Ni(II)−Fe(II) exchange at GR particle edges. The results of this study reveal GR to be a dynamic sorbent that engages in dissolution−reprecipitation and exchange reactions, causing extensive incorporation of trace metal $Ni(II)_{aq}$. Additional work is needed to further define the mechanisms involved and to assess the sorptive reactivity of GR with other trace metal species.

KEYWORDS: *iron, trace metals, layered double hydroxides, suboxic environments, sorption, precipitation, X-ray absorption spectroscopy, X-ray diffraction*

INTRODUCTION

Green rust (GR) minerals are mixed-valent iron (Fe) phases in the layered double hydroxide (LDH) mineral family.[1] They are composed of brucitic $Fe^{II}(OH)_2$ sheets in which part of the ferrous (divalent) Fe cations have been replaced with ferric (trivalent) Fe. This substitution generates a positive structural charge in the mineral layers, which is balanced by the coordination of anions such as carbonate (CO_3^{2-}), sulfate (SO_4^{2-}), and chloride (Cl^-) anions along the basal planes bounding the hydrated interlayer space. The resulting minerals are referred to as anionic clays and have the chemical formula $Fe^{II}_{1-x}Fel^{III}_{x}$ $(OH)_2(A^{n-})_{x/n}$. nH_2O, where A is the interlayer anion and x represents the molar fraction of trivalent Fe, which typically ranges from 0.25 to 0.33.[1−4]

Its open, hydrated structure facilitates the rapid precipitation of GR, while its layered architecture gives the mineral a high specific surface area.[2,5,6] The presence of GR has been documented in a variety of natural and engineered environments, including soils, sediments, groundwater, stratified lacustrine water columns, corroding municipal drinking water lines, and Fe(0)-based permeable reactive barriers.[7−21] These systems are typified by Eh values at or near the Fe(II)−Fe(III) redox boundary (corresponding to moderately reducing conditions) and pH values in the near-neutral to slightly alkaline range. GR formation may proceed through both biotic and abiotic pathways, as discussed in the recent review of Usman *et al.*[5]

The common occurrence of GR in reducing geochemical environments combined with its high specific surface area makes this mineral a potentially major regulator of the solubility of trace elements and pollutants in these systems. The reactivity of GR has therefore attracted considerable previous interest. Most studies have focused on its redox reactivity, and these have shown that GR is a reductant of a range of compounds including metals, oxyanions, radionuclides, and chlorinated hydrocarbons.[22−42] GR additionally retains anions including carbonate, sulfate, sulfite, selenate, and halide anions in the interlayer through electrostatic interactions with the mineral basal planes[4,42−48] and may form inner-sphere complexes at amphoteric edge sites as observed for phosphate, arsenate, and arsenite.[49−52]

Studies of the interaction of GR with trace metals have addressed redox and co-precipitation reactions and have demonstrated that GR is capable of reducing Cu(II) and Hg(II)

Received: March 3, 2021
Revised: July 4, 2021
Accepted: July 6, 2021
Published: July 20, 2021

https://doi.org/10.1021/acs.est.1c01442
Environ. Sci. Technol. 2021, 55, 10411−10421

to Cu(0) and Hg(0), respectively,[32] and can incorporate an array of divalent and trivalent metal species into its structure.[53−59] There are, however, no literature reports on the interactions of pre-formed GR with trace metals that do not engage in redox reactions with the sorbent [*e.g.*, Ni(II) and Zn(II)]. This cannot be explained by a lack of environmental relevance: GR minerals and dissolved metals are likely to co-exist and interact in reducing environments such as suboxic soils, where reductive dissolution of Fe(III) oxides establishes geochemical conditions favorable to the formation of GR and leads to the release of trace metal sorbates into solution.[43,60−62] A likely factor is the difficulty of working with GR because of its high sensitivity toward oxidation, which necessitates the implementation of strict anoxic protocols to study the sorptive reactivity of the pristine GR surface. A further complication is that GR has a relatively high solubility that depends strongly on pH.[63] This makes it difficult to avoid GR dissolution and prevent co-precipitation reactions in metal sorption experiments, where pH shifts are common.

The aim of the work presented here was to characterize the reactivity of pre-formed GR as a sorbent of dissolved Ni(II), a trace metal that is redox-stable in the presence of GR. The experiments were designed to avoid net GR dissolution or precipitation during sorption and employed a combination of batch kinetic studies and spectroscopic analyses to characterize the extent and mechanisms of interaction. The results reveal that incorporation rather than surface complexation reactions dominate the reactivity of GR toward aqueous Ni(II) even in the absence of net dissolution or precipitation of the sorbent.

MATERIALS AND METHODS

Anoxic Protocols. The anoxic procedures used here were the same as those described previously.[64,65] Briefly, the experiments were conducted in an anerobic glovebox which had a 95% $N_{2(g)}$ and 5% $H_{2(g)}$ atmosphere and was equipped with a Coy fan box that continuously circulated the glovebox air over granular Pd catalyst to remove trace $O_{2(g)}$. Samples and reagents were prepared with doubly deionized water (conductivity > 18.2 MΩ cm) that had been boiled and then was left to cool inside the glovebox while open to the glovebox atmosphere. Containers and other labware were brought into the glovebox at least 24 h before use.

GR Synthesis. GR with sulfate as the charge-balancing interlayer anion (henceforth referred to as GR-sulfate or simply GR) was synthesized inside the glovebox using a procedure modified from that used by Refait *et al.*[66] This co-precipitation method involved titration of a solute containing 0.28 M $Fe(II)SO_{4(aq)}$ and 0.035 M $Fe(III)_2(SO_4)_{3(aq)}$ with 0.30 M $NaOH_{(aq)}$ in a 1:1.4 volume ratio. The resulting green−blue suspension (referred to as the "synthesis suspension" below) had a pH of 7.0 and was aged for 5 d inside the glovebox. Solids were collected by vacuum filtration and analyzed by powder X-ray diffraction (XRD) (details below). The results confirmed that the material was GR and showed no evidence of the presence of other Fe phases, as described below.

Sorption Experiments. The sorption studies were designed to minimize net dissolution or precipitation of the GR sorbent during reaction with $Ni(II)_{aq}$. To this end, the GR suspensions were pre-equilibrated before Ni(II) was added and stabilized against pH changes using Tris buffer. Tris was selected based on the findings of Yin *et al.*,[67] who reported that it did not cause GR dissolution, in contrast to the Good's buffer HEPES. The background electrolyte consisted of 0.05 M Na_2SO_4 stabilized at pH 7.8 with 10 mM Tris.

Pre-equilibration was done in two steps. In the first, a 25 mL aliquot of the GR synthesis suspension was vacuum-filtered (inside the glovebox) through a 0.2 μm nitrocellulose membrane. The moist GR deposit remaining on the filter was washed by filtering through 10 mL of anoxic background electrolyte. The filtered and washed GR material was collected and resuspended in 30 mL of anoxic electrolyte. A total of eight suspensions were prepared. Sample containers were wrapped in Al foil and equilibrated inside the glovebox for 2 d.

To start the second pre-equilibration step, the suspensions were transferred into 35 mL polypropylene centrifuge tubes. These were sealed with Nalgene caps having a polypropylene screw closure and a silicone gasket and brought outside the glovebox for centrifugation at 13,500 rpm for 10 min to achieve solid−solution separation. The centrifuged suspensions were brought back into the glovebox, where the solutes were collected and combined into a single sample of ∼240 mL, while the solids were discarded. A 150 mL volume of the solute was transferred into a separate container and amended with fresh GR that was filtered from the synthesis suspension and washed with the remainder of the centrifuged solute. This involved vacuum filtration of 25 mL aliquots of the GR synthesis suspension and washing of the filtered deposit as described above. A total of five filtered 25 mL aliquots were suspended into the 150 mL solute volume to produce a single GR suspension with a solid-phase Fe concentration of 69 mM [46 mM $Fe(II)_{(s)}$ and 23 mM $Fe(III)_{(s)}$], corresponding to a GR particle density of ∼7.3 g L^{-1}. The container holding this suspension was wrapped in Al foil and equilibrated inside the glovebox for 2 d. Suspension pH was measured regularly during this time using a double-junction pH electrode (Thermo Scientific Orion 9102DJWP). Aqueous Fe(II) levels were monitored by regular retrieval of 5 mL subsamples which were syringe-filtered through 0.22 μm nylon membranes into 15 mL tubes holding 10 μL of concentrated H_2SO_4. Dissolved Fe(II) concentrations were analyzed by inductively coupled plasma optical emission spectrometry (ICP-OES). The combined pH and $[Fe(II)]_{aq}$ measurements showed that the GR suspension reached equilibrium during the 2 d pre-equilibration time frame, as shown below.

Following pre-equilibration, the GR suspension was partitioned into two 60 mL volumes held in two separate containers. One of the containers was spiked with 0.95 mM Ni(II), while the other served as a control and received no Ni(II). Addition of Ni(II) was done under magnetic stirring by the stepwise injection of 10−30 μL aliquots of a 0.2 M $NiSO_4$ stock solution. Suspension pH was monitored between Ni(II) shots and re-adjusted to the initial value of 7.80 by small additions of 0.1 M NaOH as necessary. Suspension pH varied between 7.78 and 7.81 during this process.

Following the metal spike, the containers were wrapped in Al foil and equilibrated inside the glovebox for 7 d. Suspension pH and the concentrations of $Ni(II)_{aq}$ and $Fe(II)_{aq}$ were measured daily with the same methods as those used during pre-equilibration. The suspension pH remained essentially constant during this time period, with the measured values varying by <0.04 pH units. The GR control suspension was sampled at the same time points and in the same manner as the Ni(II)-amended suspension to assess any effects of Ni(II) sorption on GR solubility; the pH of the control suspension was constant for the experimental duration. Measurements of quality control samples and replicate analyses of individual samples indicated a precision

https://doi.org/10.1021/acs.est.1c01442
Environ. Sci. Technol. 2021, 55, 10411−10421

of ±1% and an accuracy of ±2% for the ICP analyses of $[Fe(II)]_{aq}$ and $[Ni(II)]_{aq}$.

Speciation calculations with Visual MINTEQ 3.1[68] indicated that the initial Ni(II)−GR suspensions were either oversaturated or undersaturated with respect to β-$Ni(OH)_2$ based on reported solubility product (K_{sp}) values, which range from $\log(K_{sp}) = -10.79$ to $\log(K_{sp}) = -18$.[69] To assess the potential precipitation of β-$Ni(OH)_2$ in the GR suspensions, sorption experiments were also conducted at a pH of 7.0 where this phase was undersaturated according to available K_{sp} data. The pH 7.0 system had the same GR suspension density and the same Ni(II) and Tris concentrations as the pH 7.8 experiment but a considerably higher $Fe(II)_{aq}$ level due to the strong dependence of GR solubility on pH.[63] For these experiments, a 260 mL volume of GR synthesis suspension (aged for 5 d) was amended with 52 mL of 0.06 M Tris adjusted to pH 7.0. The resulting GR suspension had dissolved Tris and $Fe(II)_{aq}$ concentrations of 10 and 48 mM, respectively, and a solid-phase Fe concentration of 69 mM, as in the pH 7.8 experiments. The suspension was equilibrated for 4 d in an Al-wrapped container inside the glovebox and then split into four separate 75 mL suspensions. Two of these were spiked with 0.95 mM $Ni(II)_{aq}$ in the same manner as that described above for the pH 7.8 experiment, while the other two were controls. The four suspensions were stored in Al-wrapped containers inside the glovebox and sampled regularly to monitor the concentrations of dissolved Ni(II) and Fe(II) over the course of 17 d using the methods described above. Suspension pH values varied by <0.03 pH units during this time.

X-ray Absorption Spectroscopy and XRD Analyses. Samples for XRD and synchrotron X-ray absorption spectroscopy (XAS) were prepared with the same procedures as those described in the previous section. Each sample had a volume of 30 mL to ensure that there was enough mineral solid for analysis. The suspensions were reacted with $Ni(II)_{aq}$ for 1-17 d, and then centrifuged to collect the GR solids. To preserve the chemical state of sorbed Ni(II), the solids were not washed or dried.

For XRD analysis, a portion of the moist solids was mixed with a small volume of glycerol inside the glovebox and then smeared as a thin film onto a low-background sample holder. XRD analysis was performed outside the glovebox using a Bruker D8 diffractometer equipped with a Cu Kα source, a Ni filter, and a LynxEye solid state detector. Data were collected over the 2θ range 5−80° with a resolution of 0.02° 2θ and a counting time of 0.5 s, requiring approximately 0.5 h per pattern. Preliminary analyses (involving comparison of XRD scans collected for GR−glycerol deposits at various time points in a 5 h time frame) confirmed that glycerol was effective in protecting GR against oxidation, consistent with previous results.[23,24,63,66,70]

For XAS analysis, the moist pastes were sealed into XAS sample holders with Kapton tape inside the glovebox. The holders were wrapped in Al foil and then individually sealed into four ziplock bags for transport to the synchrotron facility. XAS data were collected by scanning the samples at the Ni *K*-edge (8333 eV) on beamline 12BM of the Advanced Photon Source (APS) at Argonne National Laboratory and on beamline 6BM of the National Synchrotron Light Source II (NSLS-II) at Brookhaven National Laboratory. Data collection was done in fluorescence mode at room temperature using a 13-element Canberra solid-state detector at beamline 12BM (APS) and a four-element vortex silicon-drift detector at beamline 6BM (NSLS-II). Multiple scans were collected per sample to improve the signal/noise ratio. The data were processed and analyzed with WinXAS 3.1[71] combined with Athena[72] and Feff 7[73] using procedures described in the Supporting Information. The first and last scan of each sorption sample were compared carefully to check for any beam-induced changes during the measurements, which were not observed.

Several Ni reference compounds were analyzed to assist the XAS data interpretation of the sorption samples. These included the following: (1) Ni(II)-substituted GR, prepared by co-precipitation in the same manner as that of the GR sorbent (see above) but with the addition of a small amount of Ni(II), which substitutes into the Fe(II) site of the GR mineral layers to form a dilute solid solution,[74,75] referred to as Ni:GR. Two Ni:GR samples were prepared, one having a molar Ni(II):Fe(II) ratio of 1:55 (corresponding to 1.8 mol %) and the other 1:27.5 (3.6 mol %); (2) Ni(II)−Fe(III)-LDH, characterized previously by Thenuwara *et al.*[76] This compound is the Ni(II) analogue of GR, containing Ni(II) instead of Fe(II) as the divalent cation in the octahedral mineral layers; and (3) Ni(II)−Al(III)-LDH and (4) β-$Ni(OH)_2$, both described previously by Scheinost and Sparks.[77] The Ni(II)−Al(III)-LDH compound is isostructural to Ni(II)−Fe(III)-LDH but has Al(III) instead of Fe(III) as the structural trivalent cation, while β-$Ni(OH)_2$ has the same brucitic structure as that of the LDH references but contains no structural trivalent cations.

RESULTS AND DISCUSSION

XRD Results. The XRD patterns of the GR starting material, the Ni/GR reference sample with Ni(II):Fe(II) = 1:27.5, and the Ni(II)−GR sorption samples are presented in Figure 1 and demonstrate that GR was the only detectable Fe phase in all samples. The patterns are dominated by three basal plane Bragg reflections (at ∼10.9, 5.5, and 3.7 Å) which are characteristic of GR compounds having three-dimensional interlayer anions such as sulfate.[4] Smaller *hkl* reflections appear in the range 30−80° 2θ and are consistent with previously reported XRD patterns of GR-sulfate.[4,5,70,78,79] The similarity of the XRD patterns of the sorption samples and the starting phase confirms that GR was stable and did not undergo bulk phase changes in the sorption experiments. The peak positions in the patterns of the sorption samples and controls differed by ≤0.02° 2θ (the resolution of the measurement), indicating that the interaction with Ni(II) did not cause structural modifications of the GR sorbent. There is variability in the intensities of the basal reflections relative to those at 30−80° 2θ (Figure 1), which may indicate differences in the extent or ordering of GR platelet stacking or in the crystallinity of the GR platelets. However, the widths of the reflections were the same in the sorption samples and controls (see Figure S1 in the Supporting Information), indicating that the intensity differences most likely are due to the effects of preferred orientation, as observed commonly for layered minerals such as phyllosilicates.[80]

Batch Kinetic Data. Figure S2 shows the aqueous Fe(II) concentration in the pH 7.8 GR control suspension [which received no $Ni(II)_{aq}$] as a function of time from the start of the second hydration step. The results show that $[Fe(II)]_{aq}$ reaches a concentration of 0.8 mM after 1 d and remains at this level for the duration of the experiment. Suspension pH was stable at a value of 7.80 (±0.02) throughout. The GR suspension was therefore at an equilibrium with respect to the dissolution−precipitation of the GR sorbent when $Ni(II)_{aq}$ was introduced after 2 d of pre-equilibration. At pH 7.0, the aqueous Fe(II) concentration was similarly stable at the time of Ni(II) addition but at a higher level of 48 mM.

https://doi.org/10.1021/acs.est.1c01442
Environ. Sci. Technol. 2021, 55, 10411−10421

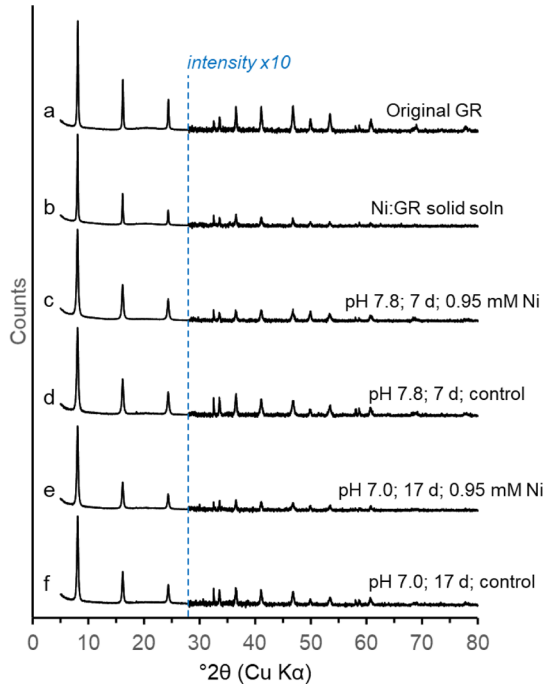

Figure 1. Powder XRD patterns of GR sorbents [patterns (a,c−f)] and the Ni-substituted GR reference with a molar Ni(II):Fe(II) ratio of 1:27.5 [pattern (b)]. Pattern (a) is of the GR starting substrate, while patterns (c,e) are of GR retrieved from the pH 7.8 and pH 7.0 sorption experiments after reaction with 0.95 mM $Ni(II)_{aq}$ for 7 d and 17 d, respectively, and patterns (d,f) are of GR collected from the corresponding control suspensions, which received no $Ni(II)_{aq}$. All patterns are dominated by the basal reflections at ∼8.1° 2θ (d ∼ 10.9 Å), ∼16.1° 2θ (d ∼ 5.5 Å), and ∼24.3° 2θ (d ∼ 3.7 Å). The regions to the high-angle side of the blue dashed line were scaled by a factor of 10 to enhance the visibility of the *hkl* bands.

The results of the batch kinetic Ni(II) sorption experiments are presented in Figure 2, with Figure 2a showing the results obtained at pH 7.8 and Figure 2b those at pH 7.0. Plotted as a function of time are the concentrations of $Ni(II)_{aq}$ and $Fe(II)_{aq}$ in the Ni(II)-amended suspensions as well as the concentration of $Fe(II)_{aq}$ in the control suspensions. At both pH values, continuous removal of $Ni(II)_{aq}$ occurs throughout the experimental reaction time frame. Sorption is initially rapid, lowering $[Ni(II)]_{aq}$ during the first hour of reaction from 0.95 to 0.67 mM at pH 7.8 and to 0.82 mM at pH 7.0. This fast initial step is followed by slow sorption, which gradually further reduces $[Ni(II)]_{aq}$ to 0.42 mM after 7 d at pH 7.8 and to 0.70 mM after 17 d at pH 7.0 (Figure 2). At both pH values, the sorption of Ni(II) appears to be still ongoing at the time of termination of the experiments (Figure 2), indicating that sorption equilibrium had not been reached in either system. The level of Ni(II) sorption is lower at pH 7.0 than that at pH 7.8 (Figure 2). This likely is the result of the higher concentrations of protons and $Fe(II)_{aq}$ at the lower pH value, making interaction of $Ni(II)_{aq}$ with the GR sorbent less favorable because of increased competition for coordination at surface sites.

In contrast to dissolved Ni(II), the concentrations of $Fe(II)_{aq}$ in the Ni(II)−GR suspensions were constant throughout the reaction time frame, remaining at the same level as that in the control suspension at both pH values (Figure 2). This indicates that the interaction with Ni(II) does not notably affect the solubility of GR, a finding that is consistent with the lack of structural change observed by XRD (Figures 1 and S1). The processes controlling Ni(II) sorption by the GR sorbent are assessed next on the basis of the Ni *K*-edge extended X-ray absorption fine structure (EXAFS) data.

EXAFS Results. The results of the Ni *K*-edge EXAFS analyses are presented in Figure 3, which shows the raw and fitted k^3-weighted χ functions of the Ni(II) sorption samples and references (Figure 3a) and the Fourier transforms (FTs) of the raw χ spectra (Figure 3b). The results of the EXAFS data fits are summarized in Table 1.

The XAS results of the Ni(II) reference compounds are a useful starting point for evaluating the data of the sorption samples. The β-Ni(OH), Ni(II)−Fe(III)-LDH, Ni(II)−Al-(III)-LDH, and Ni(II):GR references are all composed of octahedral layers with the brucite structure but contain varying

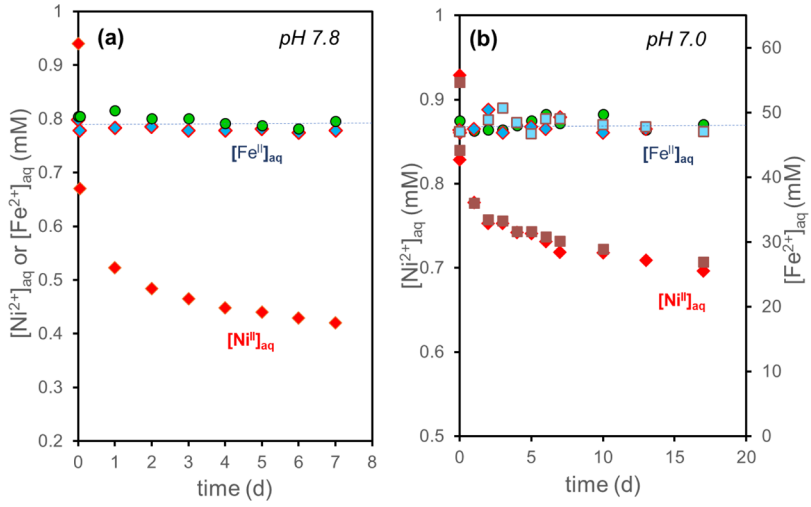

Figure 2. Results of the batch sorption kinetic experiments conducted at (a) pH 7.8 and (b) pH 7.0. The red and brown data points are the $Ni(II)_{aq}$ concentrations in the sorption samples, while the corresponding $Fe(II)_{aq}$ concentrations are represented by the blue markers. The green data points are the $Fe(II)_{aq}$ concentrations in the control suspensions, which were not spiked with $Ni(II)_{aq}$. The diamonds and squares in panel (b) are the results of duplicate experiments. The horizontal dotted lines are the average of the Fe(II)aq levels measured in the sorption and control samples (0.79 and 48.1 mM at pH 7.8 and pH 7.0, respectively). All $Fe(II)_{aq}$ concentrations are within 5.5% of the average at both pH values.

https://doi.org/10.1021/acs.est.1c01442
Environ. Sci. Technol. 2021, 55, 10411−10421

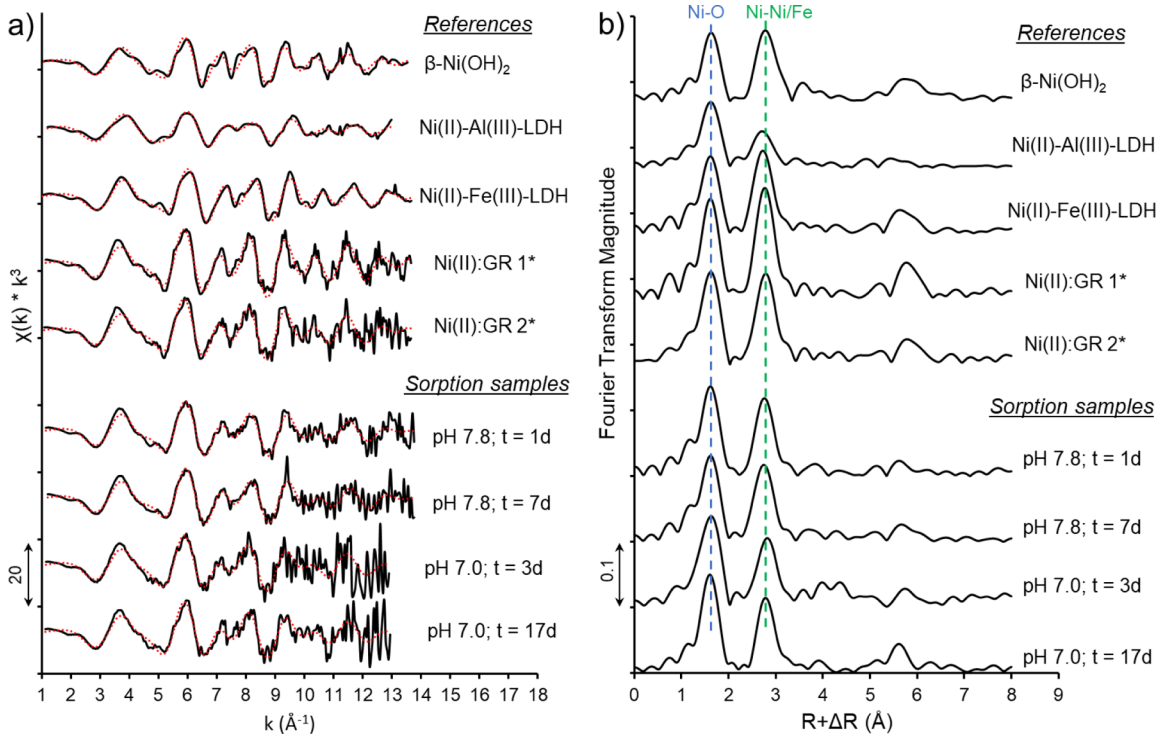

Figure 3. Ni *K*-edge EXAFS data of the sorption samples and reference compounds. Panel (a) displays the k^3-weighted χ spectra and (b) the corresponding FTs, which are uncorrected for the phase shift. The scaling of the *y*-axis is indicated by the double-arrow scale bars. The black solid and red dotted lines in panel (a) are the raw and fitted spectra, respectively, while the vertical dotted lines in panel (b) locate the first-shell O and second-shell Ni or Fe atomic neighbors surrounding sorbed Ni(II). The Ni:GR 1 and Ni:GR 2 reference compounds are Ni(II)-substituted GR phases with Ni(II):Fe(II) ratios of 1:27.5 and 1:55, respectively. The data fit results are summarized in Table 1.

Table 1. EXAFS Fit Results of the Ni(II) Reference and Sorption Samples

	Shell					
	Ni−O			Ni−Ni/Fe/Al[c]		
Sample type	$N^{a,b}$	R (Å)[a]	σ^2 (Å^2)[a]	$N^{a,b}$	R (Å)[a]	σ^2 (Å^2)[a]
References						
β-Ni(OH)$_2$	6	2.08	0.008	6 (Ni)	3.15	0.008
Ni(II)−Al(III)-LDH[d]	6	2.05	0.008	3 (Ni)	3.04	0.006
				3 (Al)	3.04	0.006
Ni(II)−Fe(III)-LDH[d]	6	2.06	0.007	3 (Ni)	3.09	0.008
				3 (Fe)	3.09	0.008
Ni:GR1[e]	6	2.06	0.004	6 (Fe)	3.15	0.005
Ni:GR2[e]	6	2.07	0.005	6 (Fe)	3.16	0.006
Sorption samples[f]						
pH 7.8; t = 1 d	6	2.06	0.006	6 (Fe)	3.14	0.008
pH 7.8; t = 7 d	6	2.06	0.006	6 (Fe)	3.13	0.008
pH 7.0; t = 3 d	6	2.06	0.005	6 (Fe)	3.16	0.008
pH 7.0; t = 17 d	6	2.06	0.005	6 (Fe)	3.15	0.009

[a]N is the coordination number, R is the radial distance, and σ^2 is the mean square relative displacement, a disorder parameter that accounts for the mean square variation in path length. The accuracies for fitted R values were estimated as ±0.01 Å for the first shell and ±0.03 Å for the second shell (see discussion in the Supporting Information), and the standard deviations of the fitted R and σ^2 values were $<\pm 6 \times 10^{-4}$ Å and $<\pm 5 \times 10^{-5}$ Å^2, respectively, in all fits. [b]Coordination numbers were fixed during fitting. [c]Second-shell atomic neighbors are indicated in brackets. [d]Values of R and σ^2 of second-shell Ni and Al in Ni(II)−Al(III)-LDH and of second-shell Ni and Fe in Ni(II)−Fe(III)-LDH were constrained to be equal. [e]The Ni:GR1 and Ni:GR2 references are Ni(II)-substituted GR phases with Ni(II):Fe(II) ratios of 1:27.5 and 1:55, respectively. [f]Fits of the sorption samples assumed positioning of Ni(II) in the octahedral Fe(II) site of the GR lattice.

levels of Ni(II) *versus* Fe(II/III) or Al(III). The structural similarity of these compounds is reflected in their similar XAS data (Figure 3). The FTs are dominated by two shells: the first at $R + \Delta R \sim 1.7$ Å representing the first-shell O ligands surrounding Ni(II) and the second at $R + \Delta R \sim 2.8$ Å representing second-neighbor Fe and Ni atoms (Figure 3b). The fit results (Table 1) show that Ni(II) is in octahedral coordination with first-shell O in all four compounds, as evidenced by the Ni−O distances (R_{Ni-O}) of 2.05−2.08 Å.[81] Second-shell Ni neighbors in β-Ni(OH)$_2$ are fitted at R_{Ni-Ni} = 3.15 Å (Table 1), consistent with previous XAS reports[77,82] and with the crystal structure of β-Ni(OH)$_2$ determined from

https://doi.org/10.1021/acs.est.1c01442
Environ. Sci. Technol. 2021, 55, 10411−10421

XRD.[83] Replacement of 1/3 of Ni(II) by Fe(III) to form Ni(II)−Fe(III)-LDH shortens the radial distance to $R_{Ni-Ni/Fe}$ = 3.09 Å (Table 1). This reflects structural contraction of the octahedral mineral sheets caused by the smaller atomic radius of Fe(III) relative to that of Ni(II) (0.645 Å *vs* 0.69 Å).[81] Incorporation of Al(III) (0.535 Å)[80] in Ni(II)−Al(III)-LDH contracts the structure further, as evidenced by the second-shell radial distance $R_{Ni-Ni/Al}$ = 3.04 Å fitted for this compound (Table 1), which is a value consistent with previous studies.[77,82,84]

The fit results of the Ni(II):GR solid solution samples show that the substitution of Ni(II) as an impurity in the Fe(II) site of the GR lattice yields a R_{Ni-Fe} of 3.15−3.16 Å (Table 1), which is very similar to R_{Ni-Ni} = 3.15 Å in β-$Ni(OH)_2$ but shorter than the interatomic Fe−Fe distance in GR (R_{Fe-Fe} = 3.21 Å[64]). The structural contraction around incorporated Ni(II) impurities reflects the smaller atomic radius of octahedral Ni(II) relative to that of Fe(II) (0.69 Å *vs* 0.78 Å[81]) and suggests considerable flexibility of the structure in accommodating Ni(II) substitution, which likely is the result of the two-dimensional architecture of the mineral lattice. Overall, the EXAFS data of the reference compounds demonstrate similar local coordination environments of Ni(II) in GR, β-$Ni(OH)_2$, and Ni(II)−Fe(III)-LDH (Figure 3; Table 1). This limits the ability of Ni K-edge XAS to reliably distinguish between these phases, particularly since the technique cannot differentiate between Ni and Fe atomic neighbors owing to their similar backscattering behaviors.[85]

The fit results of the Ni(II)−GR sorption samples show that sorbed Ni(II) is octahedral (R_{Ni-O} = 2.07 Å; Table 1). The FTs of the sorption samples (Figure 2b) display second-shell peaks with intensities that are considerably higher than those observed in XAS studies of Ni(II) inner-sphere surface complexes formed on goethite and hematite.[86,87] The second-shell metal neighbors are located at distances of 3.13−3.16 Å from central Ni (Table 1), which is similar to the second-neighbor distances in the β-$Ni(OH)_2$ and Ni:GR solid solution references ($R_{Ni-Ni/Fe}$ = 3.15−3.16 Å; Table 1). Precipitation of β-$Ni(OH)_2$ is ruled out as a significant process based on the similarity of the XAS data obtained at pH 7.8 [where β-$Ni(OH)_2$ is potentially supersaturated] and pH 7.0 [where β-$Ni(OH)_2$ is undersaturated; Figure 3; Table 1]. The results therefore suggest that Ni is incorporated in the octahedral sheets of GR, occupying the Fe(II) site.

Although the XAS results indicate generally similar coordination environments of sorbed and incorporated Ni(II), the intensity of the second-shell scattering is lower in the sorption samples than in the Ni:GR references (Figure 3), which is reflected in the higher fitted values of second-shell σ^2 (the mean square relative displacement; Table 1). This indicates that sorbed Ni(II) has, on average, a higher degree of structural disorder and/or a lower number of second-shell atomic neighbors than substituted Ni(II). A possible explanation is that sorbed Ni(II) may be buried in the surface region of the GR lattice and therefore displays a disordered or incomplete second-shell coordination. Another possibility is that sorbed Ni(II) forms physical or chemical mixtures of structurally similar Ni(II)-LDH phases. Of interest in this respect is Ni(II)−Fe(III)-LDH, the Ni(II) analogue of GR. The EXAFS results suggest that Ni(II)−Fe(III)-LDH is not the main Ni(II) sorption product (Table 1; Figure 3). However, the difference in fitted second-shell *R* values between the Ni(II)−Fe(III)-LDH reference and the sorption samples ($R_{Ni-Fe/Ni}$ = 3.09 Å *vs* R_{Ni-Fe} = 3.13−3.16 Å; Table 1) is near or within the estimated margin of uncertainty (±0.03 Å; see the Supporting Information). The presence of Ni(II)−Fe(III)-LDH in the sorption samples can therefore not be excluded, particularly if it coexists with Ni(II)-substituted GR in a physical mixture of these two phases. Moreover, because of the structural similarity of Ni/GR and Ni(II)−Fe(III)-LDH, it is likely that Ni(II) is capable of forming Ni(II)-LDH phases with compositions intermediate between Ni(II)-substituted GR and Ni(II)−Fe(III)-LDH. Such chemical mixing would lead to increased structural disorder, which is consistent with the XAS results but is otherwise difficult to characterize with this technique because of the similarity of second-neighbor Ni and Fe backscattering and the uncertainty in fitted second-shell $R_{Ni-Ni/Fe}$ values.

Overall, the XAS data indicate that sorbed Ni(II) is incorporated as an impurity in the GR mineral lattice or forms physical or chemical mixtures of Ni-substituted GR and secondary Ni(II)−Fe(III)-LDH. The general formula of sorbed Ni(II) can thus be summarized as $Fe^{II}_{0.67-x}Ni^{II}_{x}Fe^{III}_{0.33}(OH)_2(SO_4)_{0.165}$, where the value of x ($0 < x < 0.67$) is poorly constrained due to the similarity in XAS data of Ni(II)-LDH phases noted above. Despite this ambiguity, the data unequivocally demonstrate that Ni(II) is incorporated into the octahedral layers of a mixed-valent Fe(II/III)-LDH phase during sorption and rule out the formation of mononuclear surface complexes as a major mechanism. Precipitation is consistent with the slow continuous removal of $Ni(II)_{aq}$ observed macroscopically (Figure 2) but is remarkable because it occurs under conditions of apparent equilibrium with respect to the solubility of the GR sorbent, that is, in the absence of net GR dissolution or precipitation (Figure 2). The possible pathways involved are discussed next.

Mechanisms of Ni(II) Precipitation during Sorption. Several processes may be responsible for the formation of $Fe^{II}_{0.67-x}Ni^{II}_{x}Fe^{III}_{0.33}(OH)_2$ observed here during sorption of Ni(II) on GR. The first potential mechanism involves the exchange of structural Fe(II) exposed at the GR surface by chemically similar Ni(II), placing Ni(II) in a chemical environment similar to that of the Ni(II):GR and Ni(II)−Fe(III)-LDH references. Homovalent cation exchange between Fe(II) and Ni(II) is expected to occur at the edges of the GR mineral layers where the lattice is disrupted and not along the chemically stable basal planes. The available Fe(II) exchange sites can be estimated from the shape and size of GR particles and the crystallography of the mineral layers. Transmission electron microscopy analyses of GR-sulfate synthesized with the co-precipitation method used here have shown that the mineral particles are hexagonal plates with diameters of 50−500 nm.[88−90] Assuming regular hexagons and an interatomic Fe−Fe distance of 3.21 Å,[64] the total number of Fe atoms in a 50 nm particle is calculated to be 18,431, of which 312 are present as Fe(II) along the particle edges (see the Supporting Information for calculation details); this corresponds to 1.7% of structural Fe being available for cation exchange. The same calculation for particles with a diameter of 500 nm yields an estimated exchangeability of 0.17% of total Fe. In the mineral suspension of the sorption studies, the concentration of Fe(s) present in the GR sorbent was 69 mM. Therefore, the minimum concentration of exchangeable Fe(II) was 0.12 mM, while the maximum concentration was 1.2 mM. These concentrations compare to 0.95 mM of Ni(II) added to the suspension, of which ∼0.5 mM is removed by sorption over 7 d at pH 7.8 and ∼0.2 mM over 17 d at pH 7.0 (Figure 2). Exchange of Ni(II) for lattice Fe(II) exposed at the GR surface may therefore contribute significantly

https://doi.org/10.1021/acs.est.1c01442
Environ. Sci. Technol. 2021, 55, 10411−10421

to the formation of $Fe^{II}_{0.67-x}Ni^{II}_{x}Fe^{III}_{0.33}(OH)_2$ observed experimentally. Since $[Fe(II)]_{aq}$ is stable (Figure 2), this process would need to be accompanied by re-adsorption or reprecipitation of exchanged Fe(II).

The second potential mechanism for Ni(II) incorporation is redox-driven dissolution−reprecipitation of the GR sorbent mediated by aqueous Fe(II). Steady-state mineral recrystallization has been demonstrated for the ferric oxides goethite and hematite as well as for mixed-valent magnetite when these minerals are present in anoxic solutions containing aqueous Fe(II).[91−99] In these systems, the minerals continuously dissolve and reprecipitate as the result of interfacial electron transfer reactions between Fe(II) and structural Fe(III) coupled to Fe atom exchange between the aqueous and solid phases. This recrystallization process occurs under apparent equilibrium conditions without observable changes in the solution chemistry or mineral structure,[91] as observed in the GR suspensions studied here. Although Fe(II)-catalyzed recrystallization has not been previously studied for GR, this mixed-valent Fe mineral contains substantial structural Fe(III) and may therefore well be subject to redox-driven dissolution−reprecipitation through reactions with aqueous Fe(II), which was present in the experimental suspensions at substantial (millimolar level) concentrations (Figure 2). Continuous recrystallization of the GR sorbent would facilitate the substitution of Ni(II) into Fe(II) sites of the GR structure, generating dilute Ni(II)−GR solid solutions with Ni(II) impurities distributed throughout the lattice. In the current experiments, the maximum achievable level of Ni(II) substitution amounts to 2 mol % of lattice Fe(II). This low substitution level would explain the lack of bulk structural changes observed by XRD (Figure 1), as well as the lack of change in solubility (and hence stability) of the Ni(II)-reacted phase relative to that of pure GR observed in sorption experiments (Figure 2).

The final potential mechanism for the observed formation of $Fe^{II}_{0.67-x}Ni^{II}_{x}Fe^{III}_{0.33}(OH)_2$ involves supersaturation and subsequent precipitation of these secondary phases upon Ni(II) introduction into the GR suspension. This may occur if the Ni(II) analogue of GR [*i.e.*, Ni(II)−Fe(III)-LDH] has a lower solubility than the GR sorbent itself [Fe(II)−Fe(III)-LDH]. If this is the case, the introduction of $Ni(II)_{aq}$ into pre-equilibrated GR suspensions at a level equivalent to that of $Fe(II)_{aq}$ (as done in the current experiments) may trigger dissolution of the GR sorbent to form more stable Ni(II)−Fe(III)-LDH. The potential significance of this pathway is demonstrated by the results of a recent thermodynamic study where the solubility product of Ni(II)−Al(III)-LDH was found to be approximately 2 orders of magnitude lower than that of Fe(II)−Al(III)-LDH.[100] Although no equivalent studies exist for Me(II)−Fe(III)-LDH phases, it is reasonable to assume that similar differences in solubility apply because of their structural similarity to Me(II)−Al(III)-LDH.[100] Consequently, supersaturation with respect to Ni(II)−Fe(III)-LDH may induce precipitation as observed experimentally. Given the lack of change in $[Fe(II)]_{aq}$ (Figure 2), Fe(II) released by partial GR dissolution during this process would either co-precipitate with the secondary Ni(II) phases or re-adsorb onto the GR sorbent. The amount of secondary Ni(II) phases formed by this process would be small compared to that of the GR sorbent, making detection by bulk XRD (Figure 1) difficult.

The lack of disruption of the GR dissolution−precipitation equilibrium during Ni(II) sorption {as evidenced by the stable pH and $[Fe(II)]_{aq}$ values of the Ni(II)−GR suspensions; Figure 2} provides a constraint on the processes involved in Ni(II)-LDH formation as it requires re-adsorption or reprecipitation of Fe(II) released during the exchange and GR dissolution mechanisms described above. To determine the capacity of the GR sorbent in removing excess $Fe(II)_{aq}$, a pre-equilibrated GR suspension, prepared in a similar fashion to that of the pH 7.8 Ni(II) sorption experiment of Figure 2a, was spiked with 1.0 mM $Fe(II)_{aq}$ and subsequently sampled over the course of 1 week to monitor the fate of added Fe(II). The results are displayed in Figure S4. The pH value (7.9) and $[Fe(II)]_{aq}$ level (0.9 mM) of the pre-equilibrated suspension were similar to that of the Ni(II) sorption experiment of Figure 2a and remained unchanged in the control samples during the 7 d reaction time period (Figure S4). In the Fe(II)-spiked samples, the pH was constant, but $[Fe(II)]_{aq}$ dropped from the initial value of 1.9 mM to a value of 1.6 mM within 2 d and remained at this level for the remainder of the experiment (Figure S4). The removal of ∼0.3 mM added $Fe(II)_{aq}$ is notably lower (∼40%) than the removal of ∼0.5 mM $Ni(II)_{aq}$ in the Ni(II) sorption experiment at pH 7.8 (Figure 2a). This suggests that Ni(II)−Fe(II) cation exchange is not the sole pathway of Ni(II) sorption in this system. This conclusion is consistent with the slow continuous removal of $Ni(II)_{aq}$ observed macroscopically (Figure 2), which contrasts with the fast equilibration times (minutes−hours) that are typical of cation-exchange reactions at mineral−water interfaces.[101] The combined results of these experiments therefore indicate that dissolution−reprecipitation of the GR sorbent plays a significant role in mediating Ni(II) sorption in the GR suspensions.

The dynamic behavior of GR as a sorbent of $Ni(II)_{aq}$ is driven either by solubility differences with Ni(II) or by coupled electron- and atom-exchange reactions with Fe(II), as discussed above. Differentiation between these mechanisms is not possible with the current data because of the difficulty in distinguishing between Ni(II)-LDH compounds using Ni K-edge EXAFS data noted previously (Figure 2; Table 1). A further complicating factor is that the various pathways of Ni(II) sorption may operate alongside or in concert with each other, making distinctions difficult. It is, for example, quite conceivable and perhaps even likely that sorption of Ni(II) through cation exchange precedes co-precipitation, with cation exchange dominating the initial fast stage of Ni(II) sorption and precipitation the subsequent slow stage (Figure 2). A further consideration is that Fe(II)-catalyzed GR recrystallization may not only promote Ni(II) substitution in the GR lattice but also the formation of Ni(II)-rich secondary Ni(II)−Fe(III)-LDH phases, which themselves may be subject to Fe(II)-driven recrystallization affecting their composition and stability. The importance of the individual sorption processes and their interplay may vary with experimental variables such as pH, concentration, and reaction time, adding to the complexity. Further work is needed to characterize the sorption of Ni(II) onto GR in more mechanistic and kinetic detail. Measurement of the cycling of Fe between the aqueous and solid phases using Fe isotopes to assess Fe(II)-driven recrystallization[92−99] and spatially resolved analyses of the distribution and composition of the Ni(II) phases formed during Ni(II)−GR interaction would be particularly useful to refine the operative processes. Future work will address this further.

Environmental Implications. This study provides new insights into the geochemical processes that control the solubility and speciation of Ni(II) and related trace metals in the broad array of reducing systems where GR has been

https://doi.org/10.1021/acs.est.1c01442
Environ. Sci. Technol. 2021, 55, 10411−10421

observed, which includes soils, sediments, aquifers, and municipal drinking water distribution lines. The results suggest that GR is a dynamic sorbent that interacts with $Ni(II)_{aq}$ predominantly through dissolution−reprecipitation and/or exchange reactions that lead to Ni(II) precipitation rather than through adsorption reactions that lead to the formation of mononuclear Ni(II) surface complexes. The behavior of GR as a sorbent of trace metals is therefore quite different from that of ferric oxides.[102] These findings have significant ramifications for the solubility of Ni(II) in reducing environments because precipitated trace metals typically are more strongly retained, and therefore less soluble, than surface complexes.[103] They also have implications for the development of process-based thermodynamic models of Ni(II) interactions with GR, which will require solubility products rather than complexation constants to describe prevailing retention mechanisms. Additional work is needed to further assess the mechanisms, thermodynamics, and kinetics of the processes involved and to determine whether equivalent or different reactions occur during the interaction of GR with other trace metal species.

■ ASSOCIATED CONTENT

Supporting Information

The Supporting Information is available free of charge at https://pubs.acs.org/doi/10.1021/acs.est.1c01442.

Comparison of XRD peak positions and widths in the XRD patterns of the Ni(II) sorption samples and controls; $[Fe(II)]_{aq}$ as a function of time during the second pre-equilibration step of the pH 7.8 GR suspensions; description of EXAFS data fitting procedures and discussion of the fitting parameter uncertainty; estimate of the concentration of exchangeable Fe(II) at the GR surface; and $[Fe(II)]_{aq}$ as a function of time in a pre-equilibrated GR suspension amended with 1.0 mM $Fe(II)_{aq}$ at pH 7.8 (PDF)

■ AUTHOR INFORMATION

Corresponding Author

Evert J. Elzinga − *Department of Earth & Environmental Sciences, Rutgers University, Newark, New Jersey 07102, United States;* orcid.org/0000-0003-4781-7272; Phone: +1 973 353 5238; Email: elzinga@newark.rutgers.edu

Complete contact information is available at: https://pubs.acs.org/10.1021/acs.est.1c01442

Notes

The author declares no competing financial interest.

■ ACKNOWLEDGMENTS

This research was supported by the U.S. National Science Foundation (NSF) through grant CHE-1904981. The author acknowledges Argonne National Laboratory for the use of Beamline 12BM at the Advanced Photon Source, a US Department of Energy Office of Science user facility operated for the DOE office of Science by Argonne National Laboratory under contract DE-AC02-06CH11357. The work also used beamline 6BM of the National Synchrotron Light Source II, a US Department of Energy Office of Science user facility operated for the DOE Office of Science by Brookhaven National Laboratory under contract no. DE-SC0012704. The author thanks Sungsik Lee and Benjamin Reinhart (APS 12BM) as well as Bruce Ravel (NSLS-II 6BM) for assistance with XAS data collection. The comments from three anonymous reviewers and the associate editor helped improve the manuscript and are gratefully acknowledged.

■ REFERENCES

(1) Ruby, C.; Usman, M.; Naille, S.; Hanna, K.; Carteret, C.; Mullet, M.; François, M.; Abdelmoula, M. Synthesis and Transformation of Iron-Based Layered Double Hydroxides. *Appl. Clay Sci.* **2010**, *48*, 195−202.

(2) Trolard, F.; Bourrié, G. Geochemistry of Green Rusts and Fougerite: A Reevaluation of Fe cycle in Soils. *Adv. Agron.* **2008**, *99*, 227−288.

(3) Hansen, H. C. B. Environmental Chemistry of Iron(II)-Iron(III) LDHs (Green Rusts). *Layered Double Hydroxides: Present and Future*; Nova Science Publishers: Huntington, NY, 2001; pp 469−493.

(4) Christiansen, B. C.; Balic-Zunic, T.; Petit, P.-O.; Frandsen, C.; Mørup, S.; Geckeis, H.; Katerinopoulou, A.; Stipp, S. L. S. Composition and structure of an iron-bearing, layered double hydroxide (LDH) − Green rust sodium sulphate. *Geochim. Cosmochim. Acta* **2009**, *73*, 3579−3592.

(5) Usman, M.; Byrne, J. M.; Chaudhary, A.; Orsetti, S.; Hanna, K.; Ruby, C.; Kappler, A.; Haderlein, S. B. Magnetite and green rust: Synthesis, properties, and environmental applications of mixed-valent iron minerals. *Chem. Rev.* **2018**, *118*, 3251−3304.

(6) Usman, M.; Hanna, K.; Abdelmoula, M.; Zegeye, A.; Faure, P.; Ruby, C. Formation of green rust via mineralogical transformation of ferric oxides (ferrihydrite, goethite and hematite). *Appl. Clay Sci.* **2012**, *64*, 38−43.

(7) Trolard, F.; Génin, J.-M. R.; Abdelmoula, M.; Bourrié, G.; Humbert, B.; Herbillon, A. Identification of a green rust mineral in a reductomorphic soil by Mossbauer and Raman spectroscopies. *Geochim. Cosmochim. Acta* **1997**, *61*, 1107−1111.

(8) Génin, J.-M. R.; Bourrié, G.; Trolard, F.; Abdelmoula, M.; Jaffrezic, A.; Refait, P.; Maitre, V.; Humbert, B.; Herbillon, A. Thermodynamic equilibria in aqueous suspensions of synthetic and natural Fe(II)-Fe(III) green rusts: Occurrences of the mineral in hydromorphic soils. *Environ. Sci. Technol.* **1998**, *32*, 1058−1068.

(9) Feder, F.; Trolard, F.; Klingelhöfer, G.; Bourrié, G. In situ Mossbauer spectroscopy: Evidence for green rust (fougerite) in a gleysol and its mineralogical transformations with time and depth. *Geochim. Cosmochim. Acta* **2005**, *69*, 4463−4483.

(10) Christiansen, B. C.; Balic-Zunic, T.; Dideriksen, K.; Stipp, S. L. S. Identification of Green Rust in Groundwater. *Environ. Sci. Technol.* **2009**, *43*, 3436−3441.

(11) Bearcock, J. M.; Perkins, W. T.; Dinelli, E.; Wade, S. C. Fe(II)/Fe(III) 'Green Rust' Developed within Ochreous Coal Mine Drainage Sediment in South Wales, UK. *Min. Mag.* **2006**, *70*, 731−741.

(12) Zegeye, A.; Bonneville, S.; Benning, L. G.; Sturm, A.; Fowle, D. A.; Jones, C.; Canfield, D. E.; Ruby, C.; MacLean, L. C.; Nomosatryo, S.; Crowe, S. A.; Poulton, S. W. Green rust formation controls nutrient availability in a ferruginous water column. *Geology* **2012**, *40*, 599−602.

(13) Root, R. A.; Dixit, S.; Campbell, K. M.; Jew, A. D.; Hering, J. G.; O'Day, P. A. Arsenic sequestration by sorption processes in high-iron sediments. *Geochim. Cosmochim. Acta* **2007**, *71*, 5782−5803.

(14) Johnson, C. A.; Freyer, G.; Fabisch, M.; Caraballo, M. A.; Küsel, K.; Hochella, M. F. Observations and Assessment of Iron Oxide and Green Rust Nanoparticles in Metal-Polluted Mine Drainage within a Steep Redox Gradient. *Environ. Chem.* **2014**, *11*, 377−391.

(15) Rennert, T.; Eusterhues, K.; De Andrade, V.; Totsche, K. U. Iron Species in Soils on a Mofette Site Studied by Fe K-Edge X-Ray Absorption near-Edge Spectroscopy. *Chem. Geol.* **2012**, *332-333*, 116−123.

(16) Weatherington-Rice, J.; Bigham, J. M. Buried Pre-Illinoian-Age Lacustrine Deposits with "Green Rust" Colors in Clermont County, Ohio. *Ohio J. Sci.* **2006**, *106*, 35−44.

(17) Świetlik, J.; Raczyk-Stanisławiak, U.; Piszora, P.; Nawrocki, J. Corrosion in drinking water pipes: The importance of green rusts. *Water Res.* **2012**, *46*, 1−10.
(18) Génin, J.-M. R.; Olowe, A. A.; Benbouzid-Rollet, N. D.; Prieur, D.; Confente, M.; Resiak, B. The simultaneous presence of green rust 2 and sulfate reducing bacteria in the corrosion of steel sheet piles in the harbour area. *Hyperfine Interact.* **1992**, *69*, 875−878.
(19) Génin, J.-M. R.; Olowe, A. A.; Resiak, B.; Confente, M.; Rollet-Benbouzid, N.; L'Haridon, S.; Prieur, D. Products obtained by microbially-induced corrosion of steel in a marine environment: Role of green rust two. *Hyperfine Interact.* **1994**, *93*, 1807−1812.
(20) Kounde, B.; Raharinaivo, A.; Olowe, A. A.; Rezel, D.; Bauer, P.; Génin, J. M. R. Mossbauer characterization of the corrosion products of steel in civil works: Suspension bridge and reinforced concrete. *Hyperfine Interact.* **1989**, *46*, 421−428.
(21) Roh, Y.; Lee, S. Y.; Elless, M. P. Characterization of corrosion products in the permeable reactive barriers. *Environ. Geol.* **2000**, *40*, 184−194.
(22) Legrand, L.; El Figuigui, A.; Mercier, F.; Chausse, A. Reduction of aqueous chromate by Fe(II)/Fe(III) carbonate green rust: Kinetic and mechanistic studies. *Environ. Sci. Technol.* **2004**, *38*, 4587−4595.
(23) Williams, A. G. B.; Scherer, M. M. Kinetics of Cr(VI) reduction by carbonate green rust. *Environ. Sci. Technol.* **2001**, *35*, 3488−3494.
(24) Bond, D. L.; Fendorf, S. Kinetics and Structural Constraints of Chromate Reduction by Green Rusts. *Environ. Sci. Technol.* **2003**, *37*, 2750−2757.
(25) Hansen, H.; Guldberg, S.; Erbs, M.; Bender Koch, C. Kinetics of Nitrate Reduction by Green Rusts: Effects of Interlayer Anion and Fe(II):Fe(III) Ratio. *Appl. Clay Sci.* **2001**, *18*, 81−91.
(26) Etique, M.; Zegeye, A.; Grégoire, B.; Carteret, C.; Ruby, C. Nitrate reduction by mixed Iron (II-III) hydroxycarbonate green rust in the presence of phosphate anions: The key parameters influencing the ammonium selectivity. *Water Res.* **2014**, *62*, 29−39.
(27) Hansen, H. C. B.; Koch, C. B.; Nancke-Krogh, H.; Borggaard, O. K.; Sørensen, J. Abiotic Nitrate Reduction to Ammonium: Key Role of Green Rust. *Environ. Sci. Technol.* **1996**, *30*, 2053−2056.
(28) Loyaux-Lawniczak, S.; Refait, P.; Ehrhardt, J.-J.; Lecomte, P.; Génin, J.-M. R. Trapping of Cr by Formation of Ferrihydrite During the Reduction of Chromate Ions by Fe(II)-Fe(III) Hydroxysalt Green Rusts. *Environ. Sci. Technol.* **2000**, *34*, 438−443.
(29) Lee, W.; Batchelor, B. Abiotic Reductive Dechlorination of Chlorinated Ethylenes by Iron-Bearing Soil Minerals. 2. Green Rust. *Environ. Sci. Technol.* **2002**, *36*, 5348−5354.
(30) Erbs, M.; Bruun Hansen, H. C.; Olsen, C. E. Reductive Dechlorination of Carbon Tetrachloride using Iron(II) Iron(III) Hydroxide Sulfate (Green Rust). *Environ. Sci. Technol.* **1999**, *33*, 307−311.
(31) Latta, D.; Boyanov, M.; Kemner, K.; O'Loughlin, E.; Scherer, M. Reaction of Uranium(VI) with Green Rusts: Effect of Interlayer Anion. *Curr. Inorg. Chem.* **2015**, *5*, 156−168.
(32) O'Loughlin, E. J.; Kelly, S. D.; Kemner, K. M.; Csencsits, R.; Cook, R. E. Reduction of Ag^{I}, Au^{III}, Cu^{II}, and Hg^{II} by Fe^{II}/Fe^{III} Hydroxysulfate Green Rust. *Chemosphere* **2003**, *53*, 437−446.
(33) Myneni, S. C.; Tokunaga, T. K.; Brown, G. E. Abiotic selenium redox transformations in the presence of Fe(II,III) Oxides. *Science* **1997**, *278*, 1106−1109.
(34) Pepper, S. E.; Bunker, D. J.; Bryan, N. D.; Livens, F. R.; Charnock, J. M.; Pattrick, R. A. D.; Collison, D. Treatment of Radioactive Wastes: An X-Ray Absorption Spectroscopy Study of the Reaction of Technetium with Green Rust. *J. Colloid Interface Sci.* **2003**, *268*, 408−412.
(35) Lee, W.; Batchelor, B. Reductive Capacity of Natural Reductants. *Environ. Sci. Technol.* **2003**, *37*, 535−541.
(36) Skovbjerg, L. L.; Stipp, S. L. S.; Utsunomiya, S.; Ewing, R. C. The Mechanisms of Reduction of Hexavalent Chromium by Green Rust Sodium Sulphate: Formation of Cr-Goethite. *Geochim. Cosmochim. Acta* **2006**, *70*, 3582−3592.
(37) Pantke, C.; Obst, M.; Benzerara, K.; Morin, G.; Ona-Nguema, G.; Dippon, U.; Kappler, A. Green Rust Formation during Fe(II) Oxidation by the Nitrate-Reducing Acidovorax sp. Strain BoFeN1. *Environ. Sci. Technol.* **2012**, *46*, 1439−1446.
(38) Christiansen, B. C.; Geckeis, H.; Marquardt, C. M.; Bauer, A.; Römer, J.; Wiss, T.; Schild, D.; Stipp, S. L. S. Neptunyl (Np) interaction with green rust, $GR_{Na,SO4}$. *Geochim. Cosmochim. Acta* **2011**, *75*, 1216−1226.
(39) Bach, D.; Christiansen, B. C.; Schild, D.; Geckeis, H. TEM study of Green Rust Sodium Sulphate ($GR_{Na,\ SO4}$) Interacted with Neptunyl Ions (NpO2+). *Radiochim. Acta* **2014**, *102*, 279−289.
(40) O'Loughlin, E. J.; Kelly, S. D.; Kemner, K. M. XAFS investigation of the interactions of UVI with secondary mineralization products from the bioreduction of Fe(III) oxides. *Environ. Sci. Technol.* **2010**, *44*, 1656−1661.
(41) O'Loughlin, E. J.; Kelly, S. D.; Cook, R. E.; Csencsits, R.; Kemner, K. M. Reduction of uranium(VI) by mixed iron(II)/iron(III) hydroxide (green rust): Formation of UO2 nanoparticies. *Environ. Sci. Technol.* **2003**, *37*, 721−727.
(42) Choi, J.; Batchelor, B. Nitrate reduction by fluoride green rust modified with copper. *Chemosphere* **2008**, *70*, 1108−1116.
(43) Taylor, R. M. Formation and properties of Fe(II)-Fe(III)-hydroxy-carbonate and its possible significance in soil formation. *Clay Miner.* **1980**, *15*, 369−382.
(44) Refait, P.; Drissi, S. H.; Pytkiewicz, J.; Génin, J.-M. R. The anionic species competition in iron aqueous corrosion: Role of various green rust compounds. *Corrosion Sci.* **1997**, *39*, 1699−1710.
(45) Refait, P.; Génin, J.-M. R. The oxidation of ferrous hydroxide in chloride containing aqueous media and Pourbaix diagrams of green rust one. *Corrosion Sci.* **1993**, *34*, 797−819.
(46) Refait, P.; Simon, L.; Génin, J.-M. R. Reduction of SeO_4^{2-} Anions and Anoxic Formation of Iron(II)−Iron(III) Hydroxy-Selenate Green Rust. *Environ. Sci. Technol.* **2000**, *34*, 819−825.
(47) Bourdoiseau, J. A.; Sabot, R.; Jeannin, M.; Termemil, F.; Refait, P. Determination of Standard Gibbs Free Energy of Formation of Green Rusts and Its Application to the Fe(II−III) Hydroxy-Oxalate. *Colloids Surf., A* **2012**, *410*, 72−80.
(48) Agnel, M. I.; Grangeon, S.; Fauth, F.; Elkaïm, E.; Claret, F.; Roulet, M.; Warmont, F.; Tournassat, C. Mechanistic and thermodynamic insights into anion exchange by green rust. *Environ. Sci. Technol.* **2020**, *54*, 851−861.
(49) Jönsson, J.; Sherman, D. M. Sorption of As(III) and As(V) to siderite, green rust (fougerite) and magnetite: Implications for arsenic release in anoxic groundwaters. *Chem. Geol.* **2008**, *255*, 173−181.
(50) Wang, Y.; Morin, G.; Ona-Nguema, G.; Juillot, F.; Guyot, F.; Calas, G.; Brown, G. E. Evidence for different surface speciation of arsenite and arsenate on green rust: an EXAFS and XANES study. *Environ. Sci. Technol.* **2009**, *44*, 109−115.
(51) Bocher, F.; Géhin, A.; Ruby, C.; Ghanbaja, J.; Abdelmoula, M.; Génin, J.-M. R. Coprecipitation of Fe(II-III) hydroxycarbonate green rust stabilised by phosphate adsorption. *Solid State Sci.* **2004**, *6*, 117−124.
(52) Perez, J. P. H.; Freeman, H. M.; Brown, A. P.; van Genuchten, C. M.; Dideriksen, K.; S'ari, M.; Tobler, D. J.; Benning, L. G. Direct visualization of arsenic binding on green rust sulfate. *Environ. Sci. Technol.* **2020**, *54*, 3297−3305.
(53) Hansen, H. C. B.; Koch, C. B.; Taylor, R. M. Synthesis and characterization of cobalt (II)-iron (III) hydroxide carbonate, a layered double hydroxide belonging to the pyroaurite group. *J. Solid State Chem.* **1994**, *113*, 46−53.
(54) Roh, Y.; Lee, S. Y.; Elless, M. P.; Foss, J. E. Incorporation of radioactive contaminants into Pyroaurite-like phases by electrochemical synthesis. *Clay Clay Miner.* **2000**, *48*, 266−271.
(55) Ueda, M.; Shimada, S.; Inagaki, M. Synthesis of crystalline zinc ferrite near room temperature. *J. Mater. Chem.* **1993**, *3*, 1199−2201.
(56) Bourrié, G.; Trolard, F.; Refait, P.; Feder, F. A solid-solution model for Fe(II)-Fe(III)-Mg(II) green rusts and fougerite and estimation of their Gibbs free energies of formation. *Clay Clay Miner.* **2004**, *52*, 382−394.
(57) Refait, P.; Abdelmoula, M.; Trolard, F.; Génin, J.-M. R.; Ehrhardt, J. J.; Bourrié, G. Mossbauer and XAS Study of a Green Rust

https://doi.org/10.1021/acs.est.1c01442
Environ. Sci. Technol. 2021, 55, 10411−10421

Mineral: The Partial Substitution of Fe^{2+} by Mg^{2+}. *Am. Mineral.* **2001**, *86*, 731−739.
(58) Taylor, R. M.; McKenzie, R. M. The influence of aluminum on iron oxides. VI. The formation of Fe(II)-Al(III) hydroxy-chlorides, -sulfates, and -carbonates as new members of the pyroaurite group and their significance in soils. *Clay Clay Miner.* **1980**, *28*, 179−187.
(59) Aissa, R.; Ruby, C.; Gehin, A.; Abdelmoula, M.; Génin, J.-M. R. Synthesis by coprecipitation of Al-substituted hydroxysulphate green rust $Fe^{II}4Fe^{III}_{(2-y)}Al^{III}_{y}(OH)_{12}SO_4.nH_2O$. *Hyperfine Interact.* **2004**, *156/157*, 445−451.
(60) Ponnamperuma, F. N. The chemistry of submerged soils. *Adv. Agron.* **1972**, *24*, 29−96.
(61) Kirk, G. *The Biogeochemistry of Submerged Soils*; John Wiley & Sons, Ltd: Chichester, 2004; p 282.
(62) Borch, T.; Kretzschmar, R.; Kappler, A.; Cappellen, P. V.; Ginder-Vogel, M.; Voegelin, A.; Campbell, K. Biogeochemical redox processes and their impact on contaminant dynamics. *Environ. Sci. Technol.* **2010**, *44*, 15−23.
(63) Guilbaud, R.; White, M. L.; Poulton, S. W. Surface charge and growth of sulfate and carbonate green rust in aqueous media. *Geochim. Cosmochim. Acta* **2013**, *108*, 141−153.
(64) Zhu, Y.; Elzinga, E. J. Formation of layered Fe(II)-hydroxides during Fe(II) sorption onto clay and metal-oxide substrates. *Environ. Sci. Technol.* **2014**, *48*, 4937−4945.
(65) Elzinga, E. J. Formation of layered Fe(II)-Al(III)-hydroxides during reaction of Fe(II) with aluminum oxide. *Environ. Sci. Technol.* **2012**, *46*, 4894−4901.
(66) Refait, P.; Géhin, A.; Abdelmoula, M.; Génin, J.-M. R. Coprecipitation Thermodynamics of iron(II-III) Hydroxysulphate Green Rust from Fe(II) and Fe(III) Salts. *Corrosion Sci.* **2003**, *45*, 659−676.
(67) Yin, W.; Strobel, B. W.; Hansen, H. C. B. Amino-assited dehalogenation of carbon tetrachloride by green rust: Inhibition of chloroform production. *Environ. Sci. Technol.* **2017**, *51*, 3445−3452.
(68) Gustaffson, J. P. *Visual MINTEQ Chemical Equilibrium Model Version 3.1*; Stockholm Royal Institute of Technology (KTH): Stockholm, Sweden, 2017.
(69) Mattigod, S. V.; Rai, D.; Felmy, A. R.; Rao, L. Solubility and solubility product of crystalline $Ni(OH)_2$. *J. Solution Chem.* **1997**, *26*, 391−403.
(70) Hansen, H. C. B. Composition, stabilization, and light absorption of Fe(II)Fe(III) hydroxy-carbonate ("green rust"). *Clay Miner.* **1989**, *24*, 663−669.
(71) Ressler, T. WinXAS : A new software package not only for the analysis of energy-dispersive XAS Data. *J. Phys. IV* **1997**, *7*, C2−269.
(72) Ravel, B.; Newville, M. ATHENA, ARTEMIS, HEPHAESTUS: data analysis for X-ray absorption spectroscopy using IFEFFIT. *J. Synchrotron Radiat.* **2005**, *12*, 537−541.
(73) Ankudinov, A. L.; Rehr, J. J. Relativistic calculations of spin-dependent X-ray absorption spectra. *Phys. Rev. B: Condens. Matter Mater. Phys.* **1997**, *56*, R1712−R1716.
(74) Refait, P.; Bauer, P.; Olowe, A. A.; Génin, J. M. R. The substitution of Fe^{2+} ions by Ni^{2+} ions in the green rust 2 compound studied by Mossbauer effect. *Hyperfine Interact.* **1990**, *57*, 2061−2066.
(75) Chaves, L. H. G.; Curry, J. E.; Stone, D. A.; Chorover, J. Fate of nickel ion in (II-III) hydroxysulphate green rust synthesized by precipitation and coprecipitation. *Rev. Bras. Cienc. Solo* **2007**, *31*, 813−818.
(76) Thenuwara, A. C.; Attanayake, N. H.; Yu, J.; Perdew, J. P.; Elzinga, E. J.; Yan, Q.; Strongin, D. R. Cobalt intercalated layered Ni Fe double hydroxides for the oxygen evolution reaction. *J. Phys. Chem. B* **2018**, *122*, 847−854.
(77) Scheinost, A. C.; Sparks, D. L. Formation of layered single- and double-metal hydroxide precipitates at the mineral/water interface: a multiple-scattering XAFS analysis. *J. Colloid Interface Sci.* **2000**, *223*, 167−178.
(78) Simon, L.; François, M.; Refait, P.; Renaudin, G.; Lelaurain, M.; Génin, J.-M. R. Structure of the Fe(II-III) layered double hydroxysulphate Green Rust Two from Rietveld analysis. *Solid State Sci.* **2003**, *5*, 327−334.
(79) Bernal, J. D.; Dasgupta, D. R.; Mackay, A. L. The oxides and hydroxides of iron and their structural inter-relationships. *Clay Miner.* **1959**, *4*, 15−30.
(80) Dohrmann, R.; Rüping, K. B.; Kleber, M.; Ufer, K.; Jahn, R. Variation of preferred orientation in orientated clay mounts as a result of sample preparation and composition. *Clay Clay Miner.* **2009**, *57*, 686−694.
(81) Shannon, R. D. Revised effective ionic radii and systematic studies of interatomic distances in halides and chalcogenides. *Acta Crystallogr., Sect. A: Cryst. Phys., Diffr., Theor. Gen. Crystallogr.* **1976**, *32*, 751−767.
(82) Elzinga, E. J.; Sparks, D. L. Reaction condition effects on nickel sorption mechanisms in illite-water suspensions. *Soil Sci. Soc. Am. J.* **2001**, *65*, 94−101.
(83) Greaves, C.; Thomas, M. A. Refinement of the structure of deuterated nickel hydroxide, $Ni(OD)_2$, by powder neutron diffraction and evidence for the structural disorder in samples with high surface area. *Acta Crystallogr., Sect. A: Found. Crystallogr.* **1986**, *42*, 51−55.
(84) Siebecker, M. G.; Sparks, D. L. Structural differentiation between layered single (Ni) and double metal hydroxides (Ni-Al LDHs) using wavelet transformation. *J. Phys. Chem. A* **2017**, *121*, 6992−6999.
(85) Brown, G. E.; Calas, G.; Waychunas, G. A.; Petiau, J. X-ray absorption spectroscopy and its applications in mineralogy and geochemistry. *Rev. Mineral.* **1988**, *18*, 431−512.
(86) Arai, Y. Spectroscopic evidence for Ni(II) surface speciation at the iron oxyhydroxide-water interface. *Environ. Sci. Technol.* **2008**, *42*, 1151−1156.
(87) Flynn, E. D.; Catalano, J. G. Competitive and cooperative effects during nickel adsorption to iron oxides in the presence of oxalate. *Environ. Sci. Technol.* **2017**, *51*, 9792−9799.
(88) Freeman, H. M.; Perez, J. P. H.; Hondow, N.; Benning, L. G.; Brown, A. P. Beam-induced oxidation of mixed-valent Fe (oxyhydr)-oxides (green rust) monitored by STEM-EELS. *Micron* **2019**, *122*, 46−52.
(89) Géhin, A.; Ruby, C.; Abdelmoula, M.; Benali, O.; Ghanbaja, J.; Refait, P.; Génin, J.-M. R. Synthesis of Fe(II-III) hydroxysulphate green rust by coprecipitation. *Solid State Sci.* **2002**, *4*, 61−66.
(90) Ruby, C.; Géhin, A.; Abdelmoula, M.; Génin, J.-M. R.; Jolivet, J.-P. Coprecipitation of Fe(II) and Fe(III) cations in sulphated aqueous medium and formation of hydroxysulphate green rust. *Solid State Sci.* **2003**, *5*, 1055−1062.
(91) Gorski, C. A.; Fantle, M. S. Stable mineral recrystallization in low temperature aqueous systems: A critical review. *Geochim. Cosmochim. Acta* **2017**, *198*, 439−465.
(92) Williams, A. G. B.; Scherer, M. M. Spectroscopic evidence for Fe(II)−Fe(III) electron transfer at the iron oxide−water interface. *Environ. Sci. Technol.* **2004**, *38*, 4782−4790.
(93) Handler, R. M.; Beard, B. L.; Johnson, C. M.; Scherer, M. M. Atom exchange between aqueous Fe(II) and goethite: an Fe isotope tracer study. *Environ. Sci. Technol.* **2009**, *43*, 1102−1107.
(94) Larese-Casanova, P.; Scherer, M. M. Fe(II) sorption on hematite: New insights based on spectroscopic measurements. *Environ. Sci. Technol.* **2007**, *41*, 471−477.
(95) Rosso, K. M.; Yanina, S. V.; Gorski, C. A.; Larese-Casanova, P.; Scherer, M. M. Connecting observations of hematite (α-Fe_2O_3) growth catalyzed by Fe(II). *Environ. Sci. Technol.* **2010**, *44*, 61−67.
(96) Frierdich, A. J.; Luo, Y.; Catalano, J. G. Trace element cycling through iron oxide minerals during redox-driven dynamic recrystallization. *Geology* **2011**, *39*, 1083−1086.
(97) Frierdich, A. J.; Catalano, J. G. Controls on Fe(II)-activated trace element release from goethite and hematite. *Environ. Sci. Technol.* **2012**, *46*, 1519−1526.
(98) Gorski, C. A.; Handler, R. M.; Beard, B. L.; Pasakarnis, T.; Johnson, C. M.; Scherer, M. M. Fe atom exchange between aqueous Fe^{2+} and magnetite. *Environ. Sci. Technol.* **2012**, *46*, 12399−12407.

https://doi.org/10.1021/acs.est.1c01442
Environ. Sci. Technol. 2021, 55, 10411−10421

(99) Joshi, P.; Gorski, C. A. Anisotopic morphological changes in goethite during Fe^{2+}-catalyzed recrystallization. *Environ. Sci. Technol.* **2016**, *50*, 7315−7324.
(100) Bhattacharya, L.; Elzinga, E. A comparison of the solubility products of layered Me(II)-Al(III)-hydroxides based on sorption studies with Ni(II), Zn(II), Co(II), Fe(II) and Mn(II). *Soil Syst.* **2018**, *2*, 20.
(101) Sparks, D. L. Kinetics and mechanisms of chemical reactions at the soil mineral/water interface. In *Soil Physical Chemistry*, 2nd ed.; Sparks, D. L., Ed.; CRC Press: Boca Raton, FL, 1999; p 135−192.
(102) Sparks, D. L. Metal and oxyanion sorption on naturally occurring oxide and clay mineral surfaces. In *Environmental Catalysts*; Grassian, V., Ed.; Taylor and Francis Books Inc: Boca Raton, FL, 2005.
(103) Sparks, D. L. *Environmental Soil Chemistry*; Academic Press: San Diego, California, 2002.

https://doi.org/10.1021/acs.est.1c01442
Environ. Sci. Technol. 2021, 55, 10411−10421